Proceedings of The Canadian Society for Mechanical Engineering International Congress 2018
CSME International Congress 2018
May 27-30, 2018, Toronto, On, Canada

The Design and Validations of the Ultrasonic Tactile Sensor

Yanjun Qian
Department of Mechanical and Mechatronics
University of Waterloo
Waterloo, Canada
y32qian@uwaterloo.ca

Hyock Ju Kwon
Department of Mechanical and Mechatronics
University of Waterloo
Waterloo, Canada
hjkwon@uwaterloo.ca

Abstract— An ultrasonic tactile sensor that can measure the stiffness of the tissue was developed. By combining analytical and numerical approaches, efficient design methodology was presented. The electrical and mechanical performance of developed sensor was experimentally validated.

Ultrasonics; Tactile sensing; Equivalent circuit

I. INTRODUCTION

Pathological changes in the tissues, such as tumors, affect the tissue stiffness. It has been reported that malignant tissues are several times stiffer than normal ones [1]. In clinical diagnosis, palpation is the oldest, but still the most commonly used technique by physicians [2, 3] to determine the stiffness of target regions. While palpation is simple, it is just a qualitative assessment and the results are widely open to user interpretation. To overcome these shortcomings, various species of tactile sensors have been developed. By integrating different types of the sensing mechanisms onto the tactile probe, one can gather haptic responses from the object in standard forms and digitize them into quantitative measurement with the help of modern signal processing techniques [2, 3].

Being a direct imitation of palpation, static-force based tactile sensors are the most common types of tactile sensors. A typical design of the force-based tactile sensor can be found in the work by Sangpradit et al. [4]. They used a robotic positioning mechanism to control the sensing position and compression depths and measured the static forces with a load cell to estimate the stiffness of inclusions inside a softer phantom. The sensing mechanism is straight-forward, and the raw data is easy to comprehend. However, it can induce severe deformations on the surface of the object, which makes the method inappropriate for deformation-sensitive operations like neurosurgery. Besides, unlike the lab phantom, the real geometry of the object is usually irregular and rough, which brings tremendous challenges to the precise displacement control.

On the other hand, vibro-tactile sensors utilize resonance phenomenon, thus can be applied to force-sensitive surfaces without inducing excessive deformations. Since the vibration characteristics are very sensitive to the environment in contact with the sensor, only minimal level of force to secure the contact with the object needs be applied; hence, no excessive pressure on the target surfaces is required. One of the examples of vibro-tactile sensors is the one developed by O.A. Lindahl et al. [5]. The device was intended to measure the stiffness of the human skin. The incident vibration signal is provided by the resonant circuit and the computer collects the filtered system response gathered by the piezoelectric pick-up. Instead of controlling the compression depths, the tactile behavior is bounded by the static force, which is done mechanically by limiting the deformation of the spring.

Based on the same principle as the Lindahl's device, our vibro-tactile sensor also works at ultrasonic frequency, but with an additional horn attached to increase the quality factor of the device. The enhanced frequency selectivity of the new design gave us a chance to use other parameters, such as quality factor and/or the sharpness of the impedance sweep response to assess the change in material properties of the target.

In this paper, the design procedures of our ultrasonic tactile sensor are presented, followed by experimental validations of mechanical and electrical performance.

II. SENSOR DESIGN

Fig. 1 shows the assembly of our ultrasonic tactile sensor.

Figure 1. Full assembly of the ultrasonic tactile sensor

A commercially available Langevin-type piezoelectric transducer was employed as the vibrator. Usually, such transducer is not operated independently, but with a deliberately designed structure attached to the output end of the transducer with a stressed bolt connection. In the meantime, the additional attachment includes a design feature at its nodal section that permits contact with a peripheral structure without affecting the vibration behavior of the system.

In tactile sensing application of the ultrasonic transducer, a vibration concentrator, a horn with a decreasing radius towards the output end, can greatly improve the sensing performance. The concentrator not only reduces the contact area of the output end (gives an edge in precise measurement), but also increases the quality factor Q of the current system. As a result, it enhanced the frequency selectivity of the device and made the load-induced response changes in frequency domain obvious. Therefore, an aluminum horn that resonates longitudinally at transducer's resonance frequency (40 kHz) was fabricated and attached to the transducer with a bolt connection.

Last but not the least, as an interface between the electrical driving circuit and electro-mechanical transducer, two sets of wires were soldered onto the copper electrodes and were later clamped to the terminals of the impedance analyzer with clippers.

A. Ultrasonic Transducer

The transducer used in this research was a commercially available device designed to operate at 40 kHz (Model: HEC-1340P4BF, Honda Electronics, Japan). Technical drawings are available on their website. The typical application for this unit is ultrasonic machining where mechanical losses are the major concerns. This ensures that this type of piezoelectric transducer has a higher quality factor over its comparators. The power is not a critical design factor in this project, but the size is. So, the most compact model with the smallest power was selected.

B. Horn Design

The horn has a combinational shape of a step and a taper as shown in Fig. 1. Analytical derivation of precise design parameters for the horn is mathematically very challenging [6–8]. Instead, a hybrid approach was adopted in this study, i.e. initial guesses were extracted from a simple analytical model and then refine these parameters through iterative processes with the aid of FEA models.

In the initial guess stage, the horn was sketched out as a half-wavelength long stepped horn, which is a successive combination of two equally long cylinders of different diameters. Note that although a stepped horn design can be adopted for tactile sensor, it may introduce a large error between the model predictions and the actual behaviors because the continuum assumption in the pure analytical model does not hold well. To smooth the transition shape, a tapered feature was introduced to replace the step. To simplify the problem and simultaneously reduce the difficulty in machining, we have tried to avoid placing the fixture feature, the flange, at the tapered part. Next, in order to incorporate the tapered feature, we can replace the smaller end of the original design with a new cantilever stepped horn and smooth out the step with the slope afterwards (Fig. 2).

These dimensions from the analytical derivations of the simple 2D model were found according to the equivalent circuit theory based on impedance analogies as shown in Fig. 3 [9]. The electrical components' values can be derived as in (1). A MATLAB code was developed to solve for them numerically.

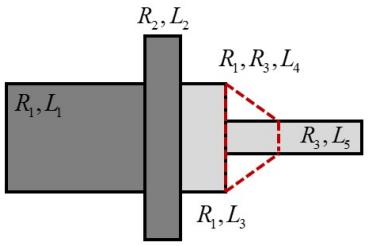

Figure 2. Design sketch for the horn: The darker grey part marks the initially designed half-wavelength (L1+L2) horn with larger diameter (R1) with the flange (R2) for fixation; The lighter grey part is the cantilever design output end (R3) with a total length of L3+L4+L5; And, finally the red dotted line shows the slope (smoothing transition from R1 to R3 in a length of L4)

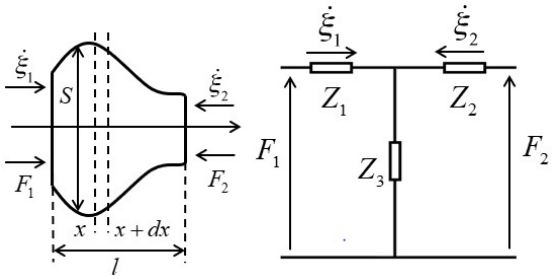

Figure 3. The analogy between the mechanical system and the corresponding electrical circuit (the impedance analogy)

$$\begin{cases} Z_1 = \dfrac{\rho c}{2jk}\left(\dfrac{\partial S}{\partial x}\right)_{x=0} + \dfrac{\rho c K S_1}{jk}\cot Kl - \dfrac{\rho c K\sqrt{S_1 S_2}}{jk\sin Kl} \\ Z_2 = -\dfrac{\rho c}{2jk}\left(\dfrac{\partial S}{\partial x}\right)_{x=0} + \dfrac{\rho c K S_2}{jk}\cot Kl - \dfrac{\rho c K\sqrt{S_1 S_2}}{jk\sin Kl}, \\ Z_3 = \dfrac{\rho c K\sqrt{S_1 S_2}}{jk\sin Kl} \end{cases} \quad (1)$$

where $K = \sqrt{k^2 - \dfrac{1}{\sqrt{S}}\dfrac{\partial^2\sqrt{S}}{\partial x^2}}$ is the generalized wave number.

In the iterative FEA simulation stage, a parametric model was constructed with a commercially validated Multiphysics package COMSOL to finalize the design with parameter sweeps. The lengthwise dimensions were tuned accordingly until the resonance frequency of the design converged within 1 kHz offset from 40 kHz. Fig. 4 shows the final design of the horn.

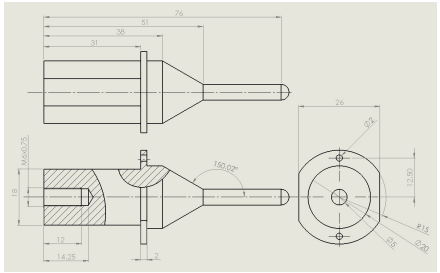

Figure 4. Final design for the horn

Identify applicable sponsor/s here. *(sponsors)*

III. EXPERIMENTAL VALIDATIONS

A. *Experiment Setups*

The first experiment was conducted to examine the mechanical behavior of fabricated horn. The test schematics is exhibited in Fig. 5.

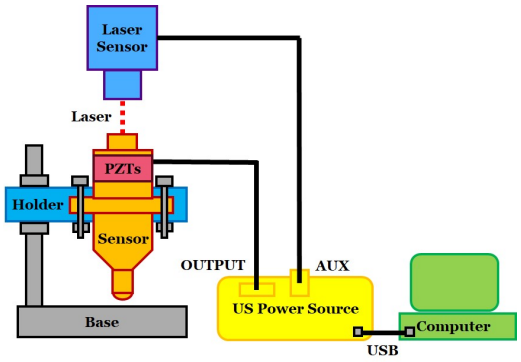

Figure 5. Test setup schematics for the design validation

A temporary holding mechanism was implemented to secure the measurement positions for the laser doppler vibrometer (Polytec OFV-505) in the experiment. The base was a bulky part made of steel, which is not sensitive to the incident vibrations generated by our sensor. The holder, made of aluminum, was fixed on the threaded pole with a set of nuts so that the height of the holder is adjustable. The sensor was fixed to the holder at its flange with two bolts. The active elements, PZTs in the transducer, were connected to the output LEMO connector on the ultrasonic power source (PDUS200, Micromechatronics, USA). The vibrometer was also connected to the power source via its auxiliary input BNC connector. The data were collected with a host computer using the controlling program for the power source via the USB connection. The actual equipment and layout are shown in Fig. 6.

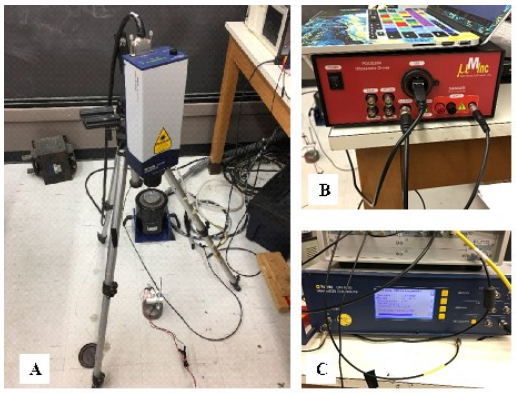

Figure 6. Actual equipment and layout of the test: A) The vibrometer head and the sensor assembly; B) The signal-collecting laptop and the ultrasonic power source; C) The vibrometer controller box

The AC signal generated by the ultrasonic power source was at the level of 20 Vpp, and the sensitivity of the laser doppler vibrometer was tuned to 1 um/V. For each measurement, a complete cycle sweep was conducted, i.e., it swept and recorded from 38 kHz to 42 kHz and then backwards. The measurement was taken on both tip end and the back of the horn as in Fig. 7.

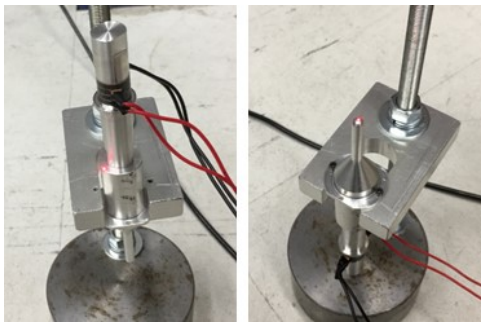

Figure 7. The laser measurement positions on the horn

The second experiment was conducted to investigate the electrical behavior of the total assembly. As discussed in the introduction, part of the designing purpose of the horn was to increase the quality factor of the sensor and thus increase the frequency selectivity. Therefore, frequency sweeps were conducted with the impedance analyzer (HP4194A) under the conditions with and without the horn.

B. *Mechanical Vibration Measurement Results*

The data collected from the experiments are plotted in Fig. 8(a) and the amplification ratio derived from Fig. 8(a) is plotted in Fig. 8(b).

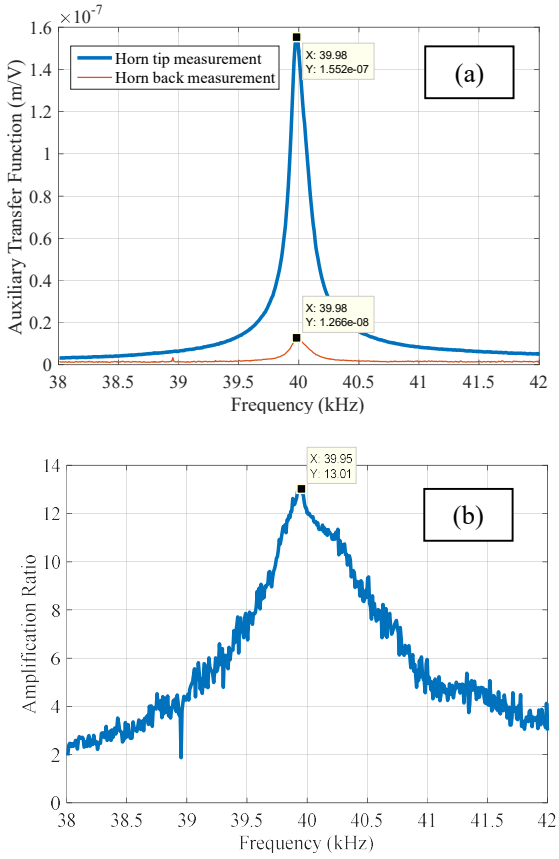

Figure 8. (a) experimental data; (b) The derived amplification ratio

The auxiliary transfer function (ratio between output voltage and auxiliary input voltage) was also automatically recorded by the embedded function in the ultrasonic power source controller program. Combining the calibration information from the laser doppler vibrometer controller box, we can find the actual transfer function ratio between the vibration magnitude (in [m]) and the input AC voltage (in [V]). It can be inferred from Fig. 8 that the system has a clear mechanical resonance at ~40 kHz (39.98 kHz to be exact).

Amplification ratio shown in Fig. 8(b) followed the similar trend to the transfer function in Fig. 8(a), and the maximum amplification ratio was 13.01 at 39.95 kHz.

C. *Electrical Measurement Results*

Fig. 9 shows the impedance and phase angle responses of the ultrasonic device with and without the horn attached.

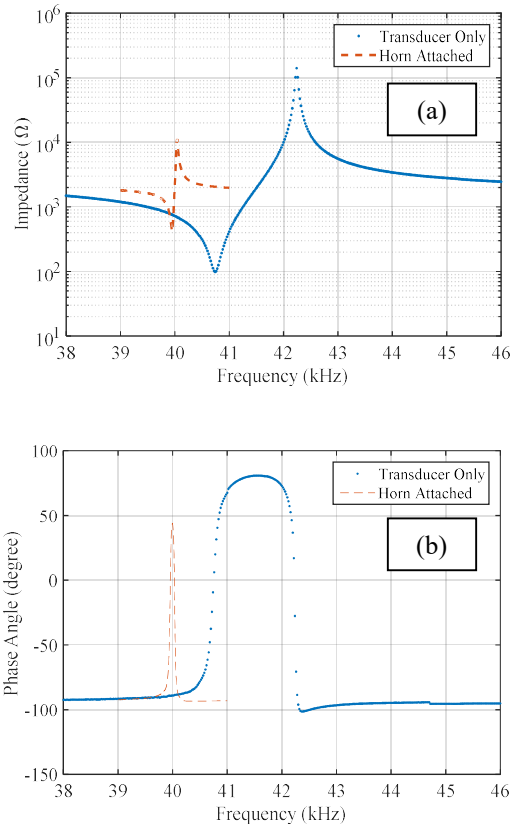

Figure 9. (a) The impedance response of the device; (b) The phase response of the device

Different ranges of frequency were used for the sweeps due to the obvious discrepancies in both responses. Both the series resonance frequency (close to the frequency where the impedance reaches minimum in Fig. 9(a) and the lower frequency where the phase angle is 0 in Fig. 9(b)) and the parallel resonance frequency (close to the frequency where the impedance reaches maximum in Fig. 9(a) and the higher frequency where the phase angle is 0 in Fig. 9(b)) shifted lower and became closer to each other (reduced difference from 2 kHz to less than 1 kHz) around 40 kHz when the horn was attached, which resulted in a steeper change from the lowest impedance to the highest impedance in Fig. 9(a) and a sharper response in the phase angle in Fig. 9(b).

D. *Comparisons and Discussions*

Table I presents the results from the analytical derivation, numerical simulation in COMSOL, and experimental measurement.

TABLE I. DATA COMPARISONS

Source	Results	
	Resonance Frequency (kHz)	***Amplification Ratio***
Analytical	40.00	>7.2
Numerical	40.61	11.4
Experimental	39.95	13.01

The experimental results show good agreement with the analytical and the numerical results. This clearly indicates that the "guess and optimize" approach is a valid way to design the current device, and mechanically, the ultrasonic sensor was working as expected.

As for the electrical responses, significant changes can be observed in Fig. 9. The responses were much "narrower" when the horn was attached to the transducer, which is a strong indication of the increase of quality factor Q, as pursued by our design.

In conclusion, the ultrasonic horn design was successfully performed through the hybrid approach by taking advantage of the modern computing power and the programable software package. By integrating the ultrasonic horn into the system, the gap between both electrical resonance frequencies was significantly reduced, which made the identification of the mechanical resonance frequency (located somewhere between two electrical resonance frequencies) more accurate and easier. The increased Q factor suggests the feasibility of using Q factor deductions as a supplementary parameter to determine the mechanical property changes in the target objects.

ACKNOWLEDGMENT

This research was supported by Natural Sciences and Engineering Research Council of Canada (NSERC).

REFERENCES

[1] E. L. Baker, J. Lu, D. Yu, R. T. Bonnecaze, and M. H. Zaman, "Cancer cell stiffness: Integrated roles of three-dimensional matrix stiffness and transforming potential," Biophys. J., vol. 99, no. 7, pp. 2048–2057, 2010.

[2] M. I. Tiwana, S. J. Redmond, and N. H. Lovell, "A review of tactile sensing technologies with applications in biomedical engineering," Sensors Actuators, A Phys., vol. 179, pp. 17–31, 2012.

[3] M. Sadeghi-Goughari, A. Mojra, and S. Sadeghi, "Parameter estimation of brain tumors using intraoperative thermal imaging based on artificial tactile sensing in conjunction with artificial neural network," J. Phys. D. Appl. Phys., vol. 49, no. 7, 2016.

[4] K. Sangpradit, H. Liu, P. Dasgupta, K. Althoefer, and L. D. Seneviratne, "Finite-element modeling of soft tissue rolling indentation," IEEE Trans. Biomed. Eng., vol. 58, no. 12 PART 1, pp. 3319–3327, 2011.

[5] O. A. Lindahl, S. Omata, and K.-A. Ängquist, “A tactile sensor for detection of physical properties of human skin in vivo,” J. Med. Eng. Technol., vol. 22, no. 4, pp. 147–153, 1998.

[6] A. Mohammed, “Equivalent circuits of solid horns undergoing longitudinal vibrations,” J. Acoust. Soc. Am., vol. 38, no. 5, pp. 862–866, 1965.

[7] S. Sherrit, B. P. Dolgin, Y. Bar-Cohen, D. Pal, J. Kroh, and T. Peterson, “Modeling of horns for sonic/ultrasonic applications,” in Ultrasonics Symposium, 1999. Proceedings. 1999 IEEE, 1999, vol. 1, pp. 647–651.

[8] S. Lin, “Study on the longitudinal-torsional composite mode exponential ultrasonic horns,” Ultrasonics, vol. 34, no. 7, pp. 757–762, 1996.

[9] Y. J. Qian, S. W. Han, and H. J. Kwon, “Development of Ultrasonic Surface Treatment Device,” in Applied Mechanics and Materials, 2016, vol. 835, pp. 620–625.